

Fitting an experimental potential energy curve for the $10(0^+)[4^3\Pi_0]$ electronic state of NaCs

Cite as: J. Chem. Phys. 151, 024307 (2019); doi: 10.1063/1.5100748

Submitted: 19 April 2019 • Accepted: 12 June 2019 •

Published Online: 12 July 2019



Andrew Steely,^{1,a)} Rachel L. Myers,^{2,b)} Andrew Kortyna,³  John Huennekens,⁴  R. F. Malenda,^{2,c)} 
and Carl Faust^{1,d)} 

AFFILIATIONS

¹Department of Physics, Susquehanna University, 514 University Ave., Selinsgrove, Pennsylvania 17870, USA

²Department of Physics and Earth Science, Moravian College, 1200 Main St., Bethlehem, Pennsylvania 18018, USA

³JILA, National Institute of Standards and Technology and University of Colorado, Boulder, Colorado 80309, USA

⁴Department of Physics, Lehigh University, 16 Memorial Drive East, Bethlehem, Pennsylvania 18015, USA

^{a)}Electronic mail: asteely@tulane.edu

^{b)}Electronic mail: stlrm08@email.arizona.edu

^{c)}Electronic mail: malendar@moravian.edu

^{d)}Electronic mail: faust@susqu.edu

ABSTRACT

We present experimentally determined potential energy curves for the $10(0^+)[4^3\Pi_0]$ electronic state of NaCs. The $10(0^+)[4^3\Pi_0]$ state exhibits a double-minimum structure, resulting in a distinctive bound-free fluorescence signature. The perturbation facilitated optical-optical double resonance method was used to obtain Doppler-free excitation spectra corresponding to rovibrational transitions to the $10(0^+)[4^3\Pi_0]$ state. Spectroscopic constants were determined to summarize data belonging to inner well, outer well, and above the barrier regions of the electronic state. The Rydberg-Klein-Rees and inverted perturbation approach methods were used to construct a potential which reproduces the experimental rovibrational energies within a root-mean-square deviation of 2.33 cm^{-1} . An alternative to the pointwise potential approach was also used to determine the potential energy curve by directly fitting an expanded Morse oscillator functional form. Advantages between the two approaches as they apply to double minimum wells are discussed.

Published under license by AIP Publishing. <https://doi.org/10.1063/1.5100748>

I. INTRODUCTION

Studies of alkali diatomic molecules are of significant interest due to many efforts to produce ultracold molecules in the lowest rovibrational levels.^{1,2} Particularly, a great deal of work in the ultracold field focuses on heteronuclear molecules.³⁻⁶ The permanent electric dipole moment of heteronuclear alkali molecules presents the possibility to orient them using an external electric field, opening opportunities for quantum computing applications.⁷⁻⁹

Many studies of NaCs, in particular, have worked toward producing accurate electronic state potential energy curves. *Ab initio* potential energy curves were computed by Korek *et al.*¹⁰ Theoretical transition dipole moment functions were calculated by Aymar and Dulieu.¹¹ An experimentally accurate potential energy curve for the ground state of NaCs was produced by Docenko *et al.*¹²

Zaharova *et al.*¹³ performed measurements and deperturbation analysis of the spin-orbit coupled $1(b)^3\Pi-2(A)^1\Sigma^+$ states. Empirical potential energy curves were also constructed for higher energies such as the $3^1\Pi$ state,¹⁴ $c^3\Sigma^+(\Omega = 1)$ state,¹⁵ $5^3\Pi_0$ state,¹⁶ and $7^1\Sigma^+$ state¹⁷ of NaCs. Some studies have used resolved bound-free fluorescence as a way to determine other molecular properties. Ashman *et al.*¹⁶ refined the repulsive wall of the $1(a)^3\Sigma^+$ state as well as determined an experimental $5^3\Pi_0 \rightarrow 1(a)^3\Sigma^+$ transition dipole moment function. Faust *et al.*¹⁷ studied the interactions between the $12(0^+)[7^1\Sigma^+]$ and $11(0^+)[5^3\Pi_0]$ states by fitting to resolved bound-free spectra and found that the two states are coupled by two separate interaction mechanisms.

From spectral data, the inverted perturbation approach (IPA)¹⁸ is commonly used to construct experimentally accurate potential energy curves.¹⁹ Although this method is straightforward, the

process of producing such a curve can be challenging when the potential of the electronic state exhibits a double minimum or shelf.²⁰ This work focuses on producing a potential energy curve for such a state, namely, the $10(0^+)[4^3\Pi_0]$ electronic state of NaCs. Note that due to the strong spin-orbit interactions present in NaCs, Hund's case (c) notation, i.e., $10(0^+)$, is most appropriate when describing electronic states; however, we will refer to the state in the more familiar Hund's case (a) notation, i.e., $4^3\Pi_0$, throughout the rest of this paper. Due to the double minimum exhibited by the $4^3\Pi_0$ state and the limitations of the IPA method for fitting to this form, a direct-potential-fit analysis was also performed with the expanded Morse oscillator (EMO) function using the betaFIT²¹ and dPotFit²² programs.

This paper is organized as follows: Section II describes the experimental setup and techniques. In Sec. III, we describe data analysis and the initial steps to fitting the potential energy curve. Section IV describes two methods for fitting the potential: the IPA pointwise method and a direct fit to an EMO functional form. Our conclusions are discussed in Sec. V.

II. THE EXPERIMENT

The experimental setup, shown in Fig. 1, is similar to that described in the work of Faust *et al.*¹⁷ Sodium and cesium metal was heated in the center of a six-armed heat pipe oven to temperatures between 260 and 310 °C. Temperature was regulated using clam shell heaters controlled by Variacs. The heated alkali metals produce atomic Na and Cs vapor, as well as molecular Na₂, Cs₂, and NaCs. Inlets near the windows of each arm allow argon gas to flow into the heat pipe to prevent the windows from being coated with alkali vapor. The region around each window was cooled by

running chilled water through copper tubes wrapped around the end of each arm. Buffer gas flow and vacuum system pumping speed were regulated to ensure that the pressure in the oven was greater than the vapor pressure of the atomic Na and Cs, usually around 3–5 Torr.

The Optical-Optical Double Resonance (OODR) technique was employed to excite transitions to high-lying electronic states in a pump-probe scheme as shown in Fig. 2. The OODR technique uses counterpropagating, narrowband, continuous wave (cw) lasers to produce Doppler-free excitation spectra. Depending on the total energy of the upper state level, one of two pump-probe laser schemes was used. For levels with total energy between about 23 800 and 24 800 cm⁻¹, the pump laser was a Toptica Photonics DL100 single mode tunable diode laser (linewidth less than 1 MHz), using a Q-Photonics QLD-840-200S laser diode. The probe laser was a Coherent 899-29 Titanium:Sapphire (Ti:Sapphire) cw ring laser (linewidth of about 500 kHz), pumped by all visible lines of a Coherent Innova 200 argon ion laser. For levels with total energy ~24 800 cm⁻¹ or higher, the Ti:Sapphire was used as the pump laser and the probe was a Coherent 699-29 cw ring dye laser (linewidth of about 500 kHz) using LDS 722 dye pumped with the 514 nm line of a Coherent Innova Sabre argon ion laser. For both schemes, the frequency of the pump laser was fixed on the pump transition, and the probe frequency was scanned while laser-induced fluorescence was detected by monitoring the anode current from a Hamamatsu R928 photomultiplier tube. The laser beams inside the heat pipe were overlapped and each focused to a spot size of approximately 1 mm diameter.

The pump laser was used to induce transitions from a thermally populated rovibrational level in the ground $1(X)^1\Sigma^+(v_X, J'' = J' \pm 1)$ state to a singlet-triplet mixed intermediate state

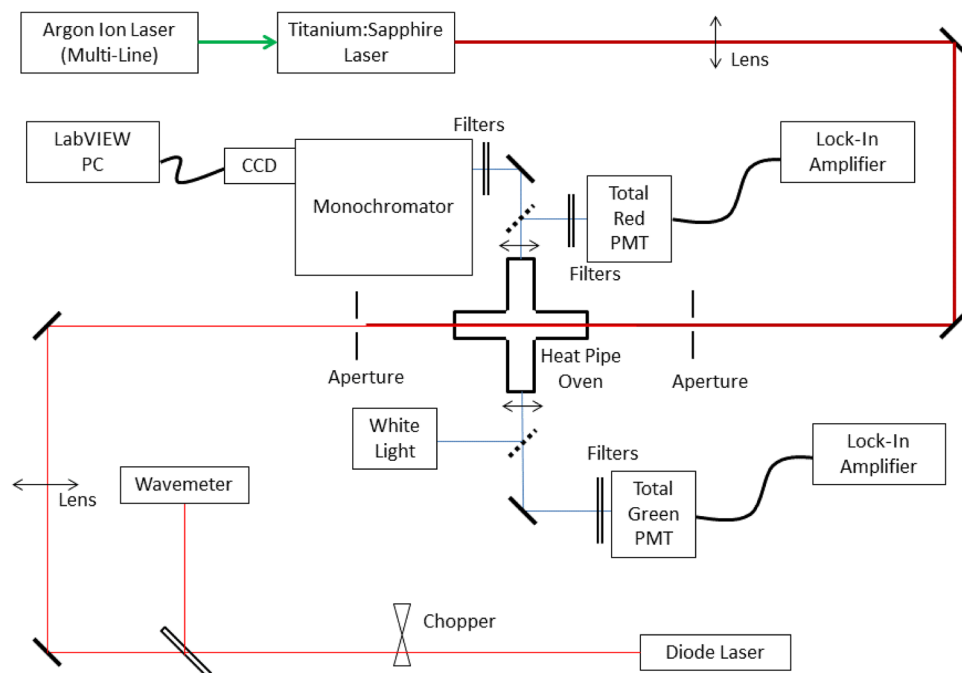


FIG. 1. Schematic diagram of the apparatus used in this work. Solid diagonal lines represent fixed mirrors, while dashed diagonal lines represent removable mirrors. Double headed arrows indicate lenses.

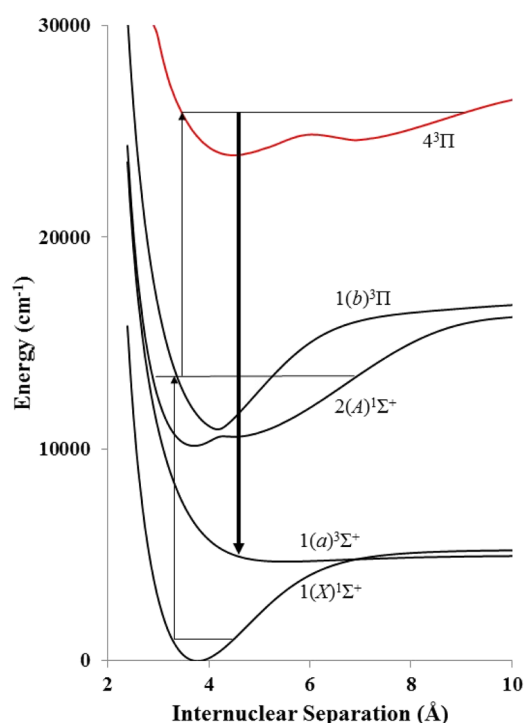


FIG. 2. Relevant theoretically calculated¹⁰ potential energy curves illustrating the pump-probe scheme used in this experiment.

$[1(b)^3\Pi(v_b, J') - 2(A)^1\Sigma^+(v_A, J')]$. Because of strong spin-orbit coupling in NaCs, these intermediate states are mixed such that every rovibrational level has significant singlet/triplet character. This allows the probe laser to induce transitions from the mixed intermediate state to upper triplet states, which would normally be inaccessible from a singlet ground state due to the spin selection rule, $\Delta S = 0$.

Double resonance transitions were observed by detecting the total fluorescence corresponding to transitions from the excited upper state down to the $1(a)^3\Sigma^+$ state as a function of probe laser frequency. The fixed-frequency laser beam was chopped and lock-in detection was used to distinguish double resonance molecular fluorescence from background noise and single laser fluorescence. Transition frequencies excited by the Ti:Sapphire laser were calibrated by comparison of its wavemeter readout to lines in a uranium atlas,²³ or to previously calibrated NaCs $2(A)^1\Sigma^+(v_A, J') \leftarrow 1(X)^1\Sigma^+(v_X, J'')$ transitions. In the former case, a small part of the Ti:Sapphire laser beam was split off into a uranium hollow cathode lamp and tuned to a particular atomic line. The Ti:Sapphire wavemeter frequency was compared to a frequency in the uranium atlas to determine the offset error of the wavemeter.

Once the Ti:Sapphire wavemeter was properly calibrated, single laser NaCs fluorescence scans could be taken and used as fingerprint markers for future calibrations. We believe that $2(A)^1\Sigma^+(v_A, J')$ level energies are determined to within $\sim 0.01 \text{ cm}^{-1}$, while level energies of electronic states accessed via double resonance are determined to an absolute accuracy of $\sim 0.02 \text{ cm}^{-1}$. The frequency of the diode laser was determined using an external Coherent RS-232

Wavemeter Wavemeter (0.001 nm resolution). Laser frequencies used by the diode laser lie close to those used by the Ti:Sapphire. This allowed us to ensure the accuracy of the external wavemeter by observing transition frequencies obtained by the diode and comparing them to those obtained from previously calibrated Ti:Sapphire scans of the same transitions. The diode laser continuously pumped the NaCs $2(A)^1\Sigma^+(v_A, J') \leftarrow 1(X)^1\Sigma^+(v_X, J'')$ transition, and its frequency was verified periodically by checking the single laser resolved bound-bound fluorescence spectrum. This was done by temporarily blocking the Ti:Sapphire beam and comparing the resulting $2(A)^1\Sigma^+(v_A, J') \rightarrow 1(X)^1\Sigma^+$ resolved fluorescence to a previously observed spectrum.

Fluorescence from either a pump laser transition or double resonance transition was resolved by focusing it onto the entrance slit of a SPEX 270M monochromator with a 600 grooves/mm diffraction grating with 1 μm blaze. The exit slit of the monochromator was replaced by a Hamamatsu charge-coupled device (CCD) array detector. The CCD detector was preferable to a photomultiplier tube (PMT) at the exit slit because it allowed for real time adjustment to account for pump laser drift, if necessary, as well as quicker assignment of upper electronic states for double resonance transitions based on resolved bound-free fluorescence to the $1(a)^3\Sigma^+$ state.

III. THE $4^3\Pi_0$ POTENTIAL

All transitions observed in double resonance excitation spectra appear as single Lorentzian peaks, regardless of which upper triplet electronic state is excited. In other studies of alkali diatomic molecules such as NaK,^{24–27} hyperfine structure can be used as a tool to identify the symmetry of upper states. However, in NaCs no such hyperfine structure is observed. Ashman *et al.*¹⁶ provide a detailed explanation of how strong spin-orbit effects account for this. As a result, resolved bound-free fluorescence must be relied upon as a means to identify which double resonance peaks correspond to particular upper triplet electronic states. Many transitions to the $4^3\Pi_0$ electronic state were studied and identified by a signature interference pattern observed in resolved bound-free spectra from these levels such as the one shown in Fig. 3. Theoretical *ab initio* calculations¹⁰ of the $4^3\Pi_0$ potential energy curve, based on nonempirical pseudopotentials taking into consideration spin-orbit effects, show that this potential likely exhibits a double minimum.

According to the classical Franck-Condon approximation,²⁸ electronic transitions occur instantaneously. This implies that during a transition, the internuclear separation, r , as well as the kinetic energy of the nuclei, does not change. By calculating the difference potential between the upper and lower states involved in bound-free fluorescence, the approximate range of wavelengths can be determined. In the case of a typical single-minimum upper state potential, a monotonic difference potential will result in a spectrum that is a simple reflection of the square of the upper state vibrational wavefunction. However, in the case of the $4^3\Pi_0$ electronic state, the difference potential is nonmonotonic, as shown in Fig. 4. Multiple values of internuclear separation contribute to transition wavelengths around 500–510 nm. This results in the interference effect observed in a typical $4^3\Pi_0$ resolved bound-free spectrum as shown in Fig. 3.

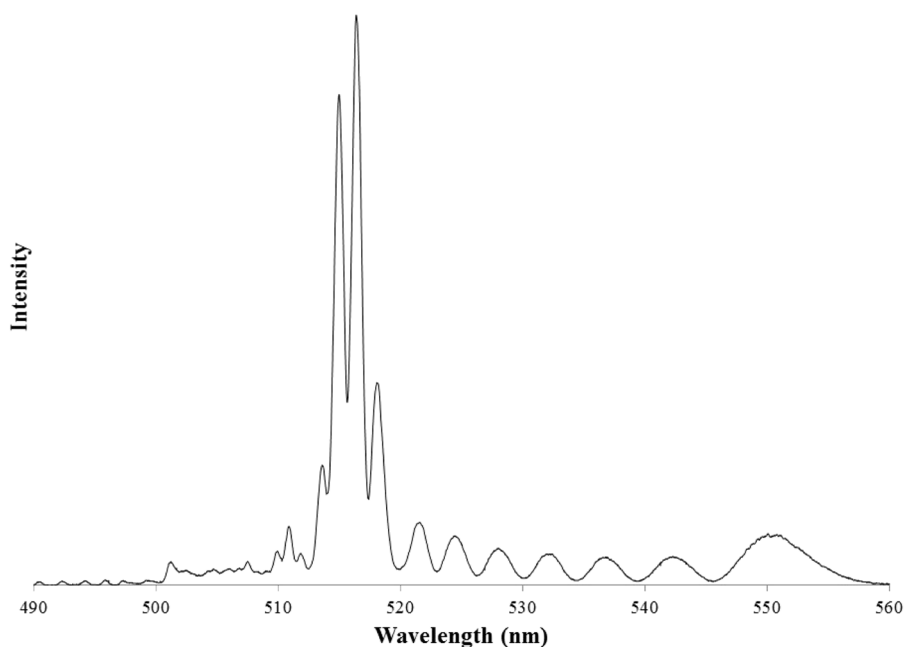


FIG. 3. Resolved bound-free $4^3\Pi_0$ ($v = 68, J = 43$) \rightarrow $1(a)^3\Sigma^+$ fluorescence spectrum. Interference observed near 515 nm acts as a signature, identifying this as fluorescence from the $4^3\Pi_0$ electronic state.

Identification of the upper state vibrational number was complicated by these interference effects. Relative numberings were used initially over separate regions as large ranges of sequential vibrational levels were identified. Most resolved bound-free fluorescence spectra appear similar to those shown in Fig. 3. However, as the dataset was expanded to the bottom of the potential well, the interference pattern disappeared for fluorescence from the lowest levels.

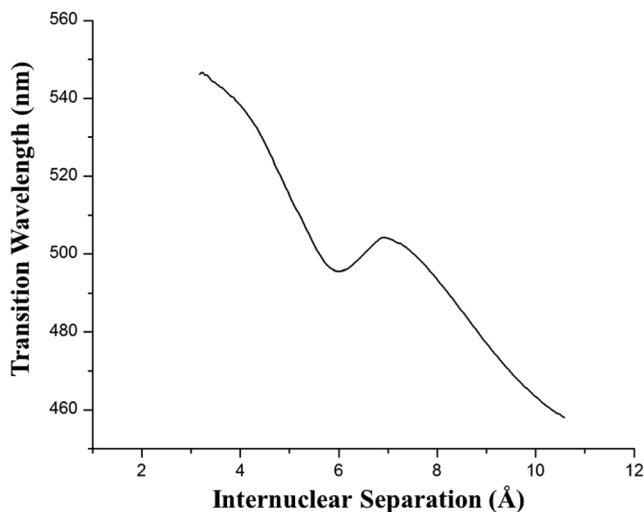


FIG. 4. Transition wavelength as a function of r , $\lambda(r) = \frac{hc}{\Delta V(r)}$, associated with the difference potential $\Delta V(r) = V_{4^3\Pi_0}(r) - V_{1(a)^3\Sigma^+}(r)$, according to the classical Franck-Condon approximation. The nonmonotonic feature (multiple r values associated with the same λ value) suggests that interference should be observed around 500 nm.

These spectra showed a clear set of countable maxima in intensity, allowing for a definite assignment of the absolute vibrational number.

Rovibrational level energy data, given in the [supplementary material](#), were organized into three distinct categories: inner well, outer well, and above the barrier regions. Data were identified as belonging to these categories based primarily on rotational spacing, but also total energy, and vibrational spacing. Levels belonging to the inner well typically have rotational constants, B_v , around 0.038 cm^{-1} , indicating an effective equilibrium internuclear separation of 4.8 \AA . Levels belonging to the outer well typically have B_v constants around 0.01 cm^{-1} , indicating an effective equilibrium internuclear separation of 9.3 \AA . Levels with energies above the barrier maximum typically have B_v constants around 0.018 cm^{-1} , indicating an effective equilibrium internuclear separation of 6.9 \AA .

A common first step for determining potential energy curves based on experimental data is to fit level energies to the Dunham expansion

$$E(v, J) = \sum_{i,k} Y_{i,k} \left(v + \frac{1}{2} \right)^i \left[J(J+1) - \Omega^2 \right]^k, \quad (1)$$

where $Y_{i,k}$ are the Dunham coefficients and $E(v, J)$ is the energy for the rovibrational level with vibrational quantum number v and rotational quantum number J . The coefficients of the expansion can then be used to determine an initial potential energy curve using the Rydberg-Klein-Rees (RKR) method.^{29–32} However, the RKR method is not effective for determining potentials with more than one minimum. Therefore, in the present case, the Dunham expansion was used to fit coefficients for the inner and outer wells of the $4^3\Pi_0$ state separately.

The dParFit16 program by Le Roy³³ from the University of Waterloo was used to determine coefficients using relative

TABLE I. Dunham coefficients for inner well and outer well regions of the $4^3\Pi_0$ electronic state as well as the rms deviations of the calculated and experimental level energies in each region. All coefficients are in units of cm^{-1} , and the number of digits reflects their statistical uncertainty.

| Inner well | | | |
|-----------------|----------|-------|-----------------------|
| $i \setminus k$ | 0 | 1 | 2 |
| 0 | 23 759.9 | 0.038 | -6.1×10^{-6} |
| 1 | 59.3 | | |
| 2 | -0.6 | | |
| rms | 2.51 | | |
| Outer well | | | |
| $i \setminus k$ | 0 | 1 | |
| 0 | 24 252 | 0.01 | |
| 1 | 22.8 | | |
| 2 | -0.47 | | |
| rms | 2.73 | | |

vibrational numbering for each region. A relatively low number of coefficients was chosen to provide a more flexible starting point for later parts of the fitting. The best fit Dunham coefficients for the inner and outer well regions, along with their respective root-mean-square (rms) deviation between the calculated and measured level energies, are given in Table I. Another program by Le Roy, RKR16,³⁴ was used to apply the RKR method to each set of Dunham coefficients, producing potential energy curves associated with the inner and outer well regions, as shown in Fig. 5. Because the vibrational numbering in the above the barrier region was not initially known and because the inner and outer well regions also have a significant effect on the radial wavefunctions in the above the barrier

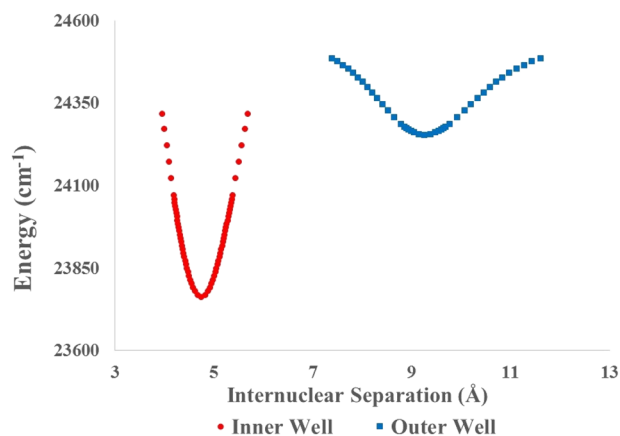


FIG. 5. RKR potentials for the NaCs $4^3\Pi_0$ inner and outer well regions. To obtain a starting point for the fitting processes, the region between these curves was interpolated using a simple functional form to construct a combined RKR potential. A simple polynomial connected the inner and outer wells. An exponential was used to extrapolate the inner wall. A simple extrapolation was used to extend the outer wall of the outer well to the $\text{Na}(3S_{1/2}) + \text{Cs}(7P_{3/2})$ dissociation limit.

region, it was not possible to apply the RKR method to the above the barrier region. However, the data do allow us to determine approximate vibrational and rotational constants, $G_v \sim 10.5 \text{ cm}^{-1}$ and $B_v \sim 0.018 \text{ cm}^{-1}$, for levels just above the barrier. To obtain a starting point for both the IPA pointwise fitting process and the direct analytical potential fitting method using dPotFit,²² the inner well and outer well curves were connected with a smooth polynomial, and the outer wall of the outer well was smoothly extrapolated to the $\text{Na}(3S_{1/2}) + \text{Cs}(7P_{3/2})$ dissociation limit.

Le Roy's LEVEL17 program³⁵ was used to calculate theoretical eigenvalues from the combined RKR curve, which were then compared to the experimental values. It was found that the RKR potential reproduced experimental energies with a relatively large rms deviation of 25.73 cm^{-1} , with most of the net deviation observed in the above the barrier region.

IV. FITTING THE $4^3\Pi_0$ POTENTIAL

A. IPA–Pointwise method

The inverted perturbation approximation (IPA) method¹⁸ can be used to iteratively adjust a potential to better reproduce experimental eigenvalues. The publicly available IPA³⁶ code, as modified by Hickman,²⁷ accepts an initial potential $V_0(r)$ and generates a first order perturbative term $V_C(r)$ such that a new potential $V(r) = V_0(r) + V_C(r)$ more accurately reproduces experimental level energies. The perturbative term is calculated on a grid by varying a set of points placed along the potential at equally spaced values of r . The program uses cubic spline interpolation to determine the behavior of the correction potential between points. The IPA program allows the user to vary the number of points used, as well as which of those points are fixed or allowed to vary. In our later iterations of IPA, certain regions of the potential were fixed to fit particular portions of the well. After each iteration, the eigenvalues of the resulting potential were calculated using LEVEL17³⁵ and compared to the experimental values. The new potential was then used as the initial potential for the next iteration of the program. This process was repeated to obtain as close a fit to the experimental data as possible. More iterations including a larger number of varied points will result in better agreement with data; however, this will typically produce a potential with unphysical characteristics such as sharp changes or wiggles in the wall of the IPA potential. The stopping point for the iterations was chosen as the best fit to the data that still maintains a simple smooth potential. The final potential resulted in an rms deviation between the fitted and measured level energies of 2.33 cm^{-1} . The final IPA potential is shown in Fig. 6 compared to the theoretically calculated potential.¹⁰ The final pointwise potential, as well as each iteration of the IPA process and its corresponding grid spacing and rms deviation of level energies, is given in the supplementary material.

The $4^3\Pi_0$ state likely interacts with neighboring electronic states through various mechanisms. The overall shape of the potential energy curve is influenced by avoided crossings with nearby electronic states of the same symmetry. The $10(0^+)$ [$4^3\Pi_0$] state likely interacts substantially with the $11(0^+)$ [$5^3\Pi_0$] state and potentially with the $12(0^+)$ [$7^1\Sigma^+$] state as discussed by Faust *et al.*,¹⁷ and resolved fluorescence from $4^3\Pi_0$ rovibrational levels also indicates transitions to the $1(X)^1\Sigma^+$ ground state. This implies that the $4^3\Pi_0$

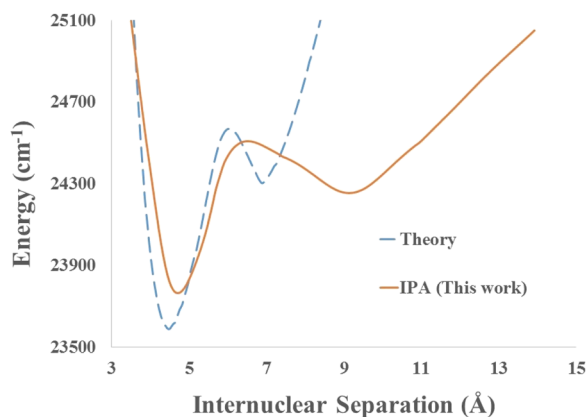


FIG. 6. The NaCs $4^3\Pi_0$ potential energy curve produced via the IPA method compared with the theoretically calculated $4^3\Pi_0$ potential of Korek.¹⁰

state also experiences spin-orbit perturbations, most likely with the nearby $6^1\Sigma^+$ state, which result in rovibrational levels having some singlet character. Because the IPA method does not include these interactions, the IPA potential has often develops gentle wiggles as a result of trying to accommodate for perturbative shifts. The potential energy curve presented here represents our best single IPA curve used to represent the experimentally determined level energies.

B. Fitting to a functional form

The EMO potential function has been shown to fit both standard single wells and potential functions with shelf or double-well features³⁷ due to additional flexibility in the exponential function

$$V_{\text{EMO}}(r) = \mathcal{D}_e \left[1 - e^{-\beta(r)(r-r_e)} \right]^2, \quad (2)$$

relative to that of the standard Morse function. Here, \mathcal{D}_e represents the well depth, r_e the equilibrium separation, and $\beta(r)$ is a power series expansion of the form

$$\beta(r) = \sum_{i=0}^{N_\beta} \beta_i \left[y_q^{\text{ref}}(r) \right]^i. \quad (3)$$

The power series is a function of $y_q^{\text{ref}}(r)$, which is a slowly varying function of the form

$$y_q^{\text{ref}}(r) \equiv \frac{r^q - r_{\text{ref}}^q}{r^q + r_{\text{ref}}^q}, \quad (4)$$

where r_{ref} is a positive reference distance greater than r_e , which allows for additional flexibility for fitting the shallow outer well, and the exponent q is a fitting parameter. While the EMO functional form is not suited to provide flexibility at long range, the experimental rovibrational data are far enough below the dissociation limit that this was not a concern for this work. In future work, if data are obtained for energies closer to the dissociation limit, another functional form, such as the Spline Exponential-Morse Long Range (SE-MLR), will be considered.

Using the betaFIT program, the combined RKR potential curve obtained as described in Sec. III was fit with the EMO function,

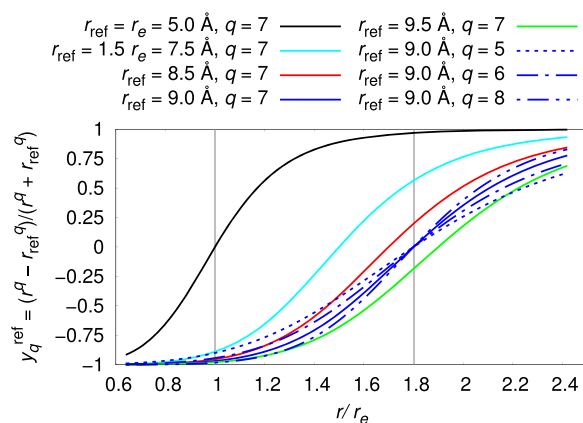


FIG. 7. Expansion variable $y_q^{\text{ref}}(r)$ given in Eq. (4) with $q = 7$ for values of $r_{\text{ref}} = r_e, 1.5 r_e, 8.5 \text{ \AA}, 9.0 \text{ \AA},$ and 9.5 \AA . For $r_{\text{ref}} = 9.0 \text{ \AA}$, $y_q^{\text{ref}}(r)$ for several values of q are compared to demonstrate how $y_q^{\text{ref}}(r)$ behaves over the region for which there are data. The positions of the primary, inner well and the secondary, outer well are represented by the left and right vertical lines, respectively.

describing the primary (inner) well using r_e for the equilibrium position and $\mathcal{D}_e = 3113.55 \text{ cm}^{-1}$ as the depth below the $\text{Na}(3S_{1/2}) + \text{Cs}(7P_{3/2})$ dissociation limit. It should be noted that the ultimate goal of this work was to reproduce the rovibrational levels determined experimentally, not to match the potential produced by the pointwise RKR fitting procedure. Thus, an iterative process was developed in which the pointwise RKR curve was given as input to the betaFIT program to determine the parameters of Eqs. (2)–(4). These parameters were then used as the input of the dPotFit program, which fits the analytical EMO form to best reproduce the rovibrational level energy data in a least squares sense. The results were then evaluated against the experimental spectral data and adjustments were made to the input parameter values of the next betaFIT calculation. This included changing the highest power of the series expansion in Eq. (3), N_β , the power q in Eq. (4), as well as the distances r_{ref} and r_e . A preliminary value of $r_e = 4.8 \text{ \AA}$ was determined using the rotational levels of the vibrational state $v = 14$, but a final value of $r_e = 5.0 \text{ \AA}$ was determined using the iterative procedure described above. The literature²¹ recommends using a value of r_{ref} of roughly 1.5 times r_e . Figure 7 shows a comparison of the function $y_q^{\text{ref}}(r)$ for several values of r_{ref} including $r_{\text{ref}} = r_e$. Due to the position of the secondary, outer well, it was found that an expansion center at a larger value of $r_{\text{ref}} = 9.0 \text{ \AA}$ was required to allow for the flexibility needed to fit this region. It was determined that using these values of $r_e = 5.0 \text{ \AA}$ and $r_{\text{ref}} = 9.0 \text{ \AA}$ in conjunction with $q = 7$ and $N_\beta = 6$ in the EMO potential produced the best agreement between the calculated energies and the experimentally measured rovibrational energies, resulting in an rms deviation of 2.53 cm^{-1} .

V. CONCLUSION

Both the pointwise method using the IPA program and direct fitting to an EMO functional form resulted in reasonable NaCs $4^3\Pi_0$ potential energy curves, as shown in Fig. 8 with rms deviations of calculated vs. experimental level energies that greatly improve upon

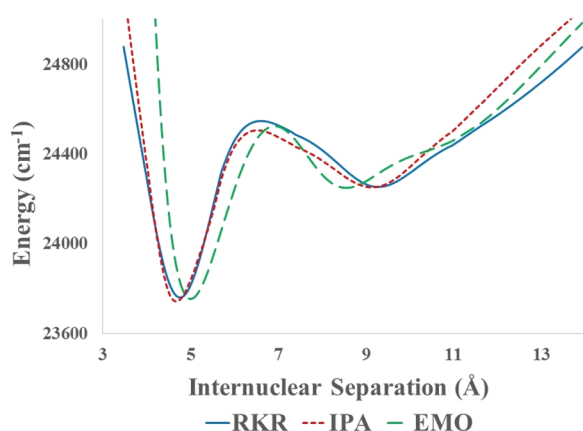


FIG. 8. Potential energy curves produced from both IPA pointwise method and direct fitting to the EMO functional form compared to the initial RKR starting curve.

the existing theoretical $4^3\Pi_0$ potential. While both methods were able to produce potential energy curves, it is clear that each has advantages and disadvantages. The IPA pointwise method allows for essentially endless flexibility in the fit since the number and location of points that are able to be varied is completely up to the user. This would be well suited to situations in which there are local perturbations such as an avoided crossing requiring that the fit be fine tuned at that location. However, the process by which IPA varies the potential points is indifferent to the physical interpretations of particular aspects of the potential curves. For example, by looking at level energies, one can determine relatively accurately what the value of r_e should be; however, choosing points for IPA to vary to accomplish this may not always be immediately obvious. This can obscure the connection between how the program is fitting and what effect it has on the final agreement with the data. This downside is eliminated by using a functional form. In many instances, the functional form has parameters that directly correlate with physical properties, making it clearer how to adjust each parameter to improve the fit. When comparing the resulting potentials produced by the two methods, it is clear that the minimum of the EMO potential is shifted compared to that of the IPA potential, in order to produce better agreement for inner well levels. Fitting to the EMO potential provides more direct control over certain aspects of the potential curve, in this case, the equilibrium separation. In this work, the $4^3\Pi_0$ potential exhibited a double-minimum, and we have found that although both methods produce similar rms deviations, fitting the potential directly to the EMO form was simpler, from a practical standpoint.

SUPPLEMENTARY MATERIAL

See [supplementary material](#) for the $4^3\Pi_0$ level energy database, final $4^3\Pi_0$ pointwise IPA potential energy curve, and final parameters for the $4^3\Pi_0$ EMO potential.

ACKNOWLEDGMENTS

This work was supported by the National Science Foundation under Grant No. PHY-1403060 at Lehigh University, and the

Summer Research Partners program at Susquehanna University. We are grateful to Professor Peet Hickman for useful discussions and to Hannah Cooper and Ciara Whipp for assistance in the lab.

REFERENCES

- W. C. Stwalley, "Efficient conversion of ultracold Feshbach-resonance-related polar molecules into ultracold ground state $X^1\Sigma^+(v=0, J=0)$ molecules," *Eur. Phys. J. D* **31**, 221–225 (2004).
- E. Shuman, J. Barry, and D. DeMille, "Laser cooling of a diatomic molecule," *Nature* **467**, 820 (2010).
- S. D. Kraft, P. Staunum, J. Lange, L. Vogel, R. Wester, and M. Weidemüller, "Formation of ultracold LiCs molecules," *J. Phys. B: At., Mol. Opt. Phys.* **39**, S993 (2006).
- C. Gabbanini and O. Dulieu, "Formation of ultracold metastable RbCs molecules by short-range photoassociation," *Phys. Chem. Chem. Phys.* **13**, 18905 (2011).
- P. Zabawa, A. Wakim, A. Neukirch, C. Haimberger, N. Bigelow, A. Stolyarov, E. Pazyuk, M. Tamanis, and R. Ferber, "Near-dissociation photoassociative production of deeply bound NaCs molecules," *Phys. Rev. A* **82**, 040501 (2010).
- A. Wakim, P. Zabawa, and N. Bigelow, "Photoassociation studies of ultracold NaCs from the $6^2P_{3/2}$ asymptote," *Phys. Chem. Chem. Phys.* **13**, 18887 (2011).
- D. DeMille, "Quantum computation with trapped polar molecules," *Phys. Rev. Lett.* **88**, 067901 (2002).
- C. Ospelkaus, S. Ospelkaus, L. Humbert, P. Ernst, K. Sengstock, and K. Bongs, "Ultracold heteronuclear molecules in a 3D optical lattice," *Phys. Rev. Lett.* **97**, 120402 (2006).
- S. Kotochigova and E. Tiesinga, "Controlling polar molecules in optical lattices," *Phys. Rev. A* **73**, 041405 (2006).
- M. Korek, S. Bleik, and A. R. Allouche, "Theoretical calculation of the low lying electronic states of the molecule NaCs with spin-orbit effect," *J. Chem. Phys.* **126**, 124313 (2007).
- M. Aymar and O. Dulieu, "Calculations of transition and permanent dipole moments of heteronuclear alkali dimers NaK, NaRb and NaCs," *Mol. Phys.* **105**, 1733 (2007).
- O. Docenko, M. Tamanis, R. Ferber, A. Pashov, H. Knöckel, and E. Tiemann, "Spectroscopic studies of NaCs for the ground state asymptote of Na + Cs pairs," *Eur. Phys. J. D* **31**, 205–211 (2004).
- J. Zaharova, M. Tamanis, R. Ferber, A. N. Drozdova, E. A. Pazyuk, and A. V. Stolyarov, "Solution of the fully-mixed-state problem: Direct deperturbation analysis of the $A^1\Sigma^+ - b^3\Pi$ complex in a NaCs dimer," *Phys. Rev. A* **79**, 012508 (2009).
- O. Docenko, M. Tamanis, J. Zaharova, R. Ferber, A. Pashov, H. Knöckel, and E. Tiemann, "High resolution spectroscopy and potential determination of the $(3)^1\Pi$ State of NaCs," *J. Chem. Phys.* **124**, 174310 (2006).
- A. Grochola, P. Kowalczyk, J. Szczepkowski, W. Jastrzebski, A. Wakim, P. Zabawa, and N. P. Bigelow, "Spin-forbidden $c^3\Sigma^+(\Omega=1) \leftarrow X^1\Sigma^+$ transition in NaCs: Investigation of the $\Omega=1$ state in hot and cold environments," *Phys. Rev. A* **84**, 012507 (2011).
- S. Ashman, B. McGeehan, C. M. Wolfe, C. Faust, K. Richter, J. Jones, A. P. Hickman, and J. Huennekens, "Experimental studies of the NaCs $5^3\Pi_0$ and $1(a)^3\Sigma^+$ electronic states," *J. Chem. Phys.* **136**, 114313 (2012).
- C. Faust, J. Jones, J. Huennekens, and R. W. Field, "Experimental studies of the NaCs $12(0^+)$ [$7^1\Sigma^+$] state: Spin-orbit and non-adiabatic interactions and quantum interference in the $12(0^+)$ [$7^1\Sigma^+$] and $11(0^+)$ [$5^3\Pi_0$] emission spectra," *J. Chem. Phys.* **146**, 104302 (2017).
- C. R. Vidal and H. Scheingraber, "Determination of diatomic molecular constants using an inverted perturbation approach: Application to the system of Mg_2 ," *J. Mol. Spectrosc.* **65**, 46–64 (1977).
- I. Birzniece, O. Nikolayeva, M. Tamanis, and R. Ferber, "Potential construction of the $B(1)^1\Pi$ state in KCs based on Fourier-transform spectroscopy data," *J. Quant. Spectrosc. Radiat. Transfer* **151**, 1–4 (2015).
- C.-C. Chu, H.-Y. Huang, T.-J. Whang, and C.-C. Tsai, "Observation of double-well potential of NaH $C^1\Sigma^+$ state: Deriving the dissociation energy of its ground state," *J. Chem. Phys.* **148**, 114301 (2018).

- ²¹R. J. Le Roy, "betaFIT: A computer program to fit pointwise potentials to selected analytic functions," *J. Quant. Spectrosc. Radiat. Transfer* **186**, 210–220 (2017), see <http://leroy.uwaterloo.ca/programs/>.
- ²²R. J. Le Roy, "dPotFit: A computer program to fit diatomic molecule spectral data to potential energy functions," *J. Quant. Spectrosc. Radiat. Transfer* **186**, 179–196 (2017), see <http://leroy.uwaterloo.ca/programs/>.
- ²³B. A. Palmer, R. Keller, and J. R. Engleman, Jr., "An atlas of uranium emission intensities in a hollow cathode discharge," LASL Report No. LA-8251-MS, 1980 (unpublished).
- ²⁴P. Burns, L. Sibbach-Morgus, A. D. Wilkins, F. Halpern, L. Clarke, R. D. Miles, L. Li, A. P. Hickman, and J. Huennekens, "The $4^3\Sigma^+$ state of NaK: Potential energy curve and hyperfine structure," *J. Chem. Phys.* **119**, 4743–4754 (2003).
- ²⁵A. D. Wilkins, L. Morgus, J. Hernandez-Guzman, J. Huennekens, and A. P. Hickman, "The NaK $1^{1,3}\Delta$ states: Theoretical and experimental studies of fine and hyperfine structure of rovibrational levels near the dissociation limit," *J. Chem. Phys.* **123**, 124306 (2005).
- ²⁶J. Huennekens, I. Prodan, A. Marks, L. Sibbach, E. Galle, T. Morgus, and L. Li, "Experimental studies of the NaK $1^3\Delta$ state," *J. Chem. Phys.* **113**, 7384–7397 (2000).
- ²⁷L. Morgus, P. Burns, R. D. Miles, A. D. Wilkins, U. Ogba, A. P. Hickman, and J. Huennekens, "Experimental study of the NaK $3^3\Pi$ double minimum state," *J. Chem. Phys.* **122**, 144313 (2005).
- ²⁸E. Condon, "The Franck-Condon principle and related topics," *Am. J. Phys.* **15**, 365–374 (1947).
- ²⁹R. Rydberg, *Z. Physik* **73**, 376 (1931).
- ³⁰R. Rydberg, *Z. Physik* **80**, 514 (1933).
- ³¹O. Klein, *Z. Physik* **76**, 226 (1932).
- ³²A. Rees, *Proc. Phys. Soc.* **59**, 998 (1947).
- ³³R. J. Le Roy, "dParFit: A computer program for fitting diatomic molecule spectral data to parameterized level energy expressions," *J. Quant. Spectrosc. Radiat. Transfer* **186**, 197–209 (2017), see <http://leroy.uwaterloo.ca/programs/>.
- ³⁴R. J. Le Roy, "RKR1: A computer program implementing the first-order RKR method for determining diatomic molecule potential energy curves," *J. Quant. Spectrosc. Radiat. Transfer* **186**, 158–166 (2017), see <http://leroy.uwaterloo.ca/programs/>.
- ³⁵R. J. Le Roy, "Level: A computer program for solving the radial Schrodinger equation for bound and quasibound levels," *J. Quant. Spectrosc. Radiat. Transfer* **186**, 167–178 (2017), see <http://leroy.uwaterloo.ca/programs/>.
- ³⁶A. Pashov, W. Jastrzebski, and P. Kowalczyk, "Construction of potential curves for diatomic molecular states by the IPA method," *Comput. Phys. Commun.* **128**, 622–634 (2000).
- ³⁷R. J. Le Roy, D. R. T. Appadoo, K. Anderson, and A. Shayesteh, "Direct-potential-fit analysis of new infrared and UV/visible $A^1\Sigma^+ - X^1\Sigma^+$ emission spectra of AgH and AgD," *J. Chem. Phys.* **123**, 204304 (2005).